Effects of V Addition on Microstructure and Hardness of Fe-C-B-Ni-V Hardfacing Alloys Cast on Steel Substrates

L. Rovatti , J.N. Lemke, A. Emami, O. Stejskal, and M. Vedani

(Submitted July 9, 2015; in revised form September 9, 2015)
Published online: 16 November 2015

1. Introduction

Hardfacing represents an effective method to deposit an hard, wear resistant material onto the surface of a relatively tough substrate in order to increase the tribological and corrosion properties of the system. This method allows to produce thick deposits up to the millimeter scale with a good metallurgical bonding with the base material. White cast irons or high-C hypereutectic alloys represent an important class of wear resistant materials that are used in applications including the mining and mineral processing, cement production, slurry pumping and pulp, and manufacturing industries (Ref 1–3). Fe-based alloys containing high volume fraction of hard phases can be employed directly as castings or as hardfacing alloys for producing thick coatings. During the deposition dilution of the coating occurs, mainly due to the diffusion of interstitial elements and to the melting of a small area of substrate during the deposition. Changes in the chemical composition induce microstructural alterations, modification of the solidification sequence and of the tribological properties of the deposit (Ref 4). Therefore, hardness and wear properties of hardfacing alloys can be optimized by chemical composition design and by microstructural control also considering the drop of interstitial elements due to diffusion toward the substrate (Ref 5). Different carbide-forming elements such as Nb, Mo, W, V, Ta, and Ti can been added to Fe-based alloys due to their strong ability to form hard phases (Ref 5, 6). In order to enhance the performance of the hardfacing alloys, it is important to select the alloying elements considering the type, morphology, and the solidification mode of the different phases they can form (Ref 7). Mo addition to high carbon Fe-based alloys can be used with the purpose of increasing the fraction of hard phases (Ref 8). A detrimental effect related to Mo addition is due to the formation of an eutectic containing Mo-rich phases (borides and carbides), in the form of an interconnected network that could facilitate the crack propagation lowering the wear resistance of the hardfacing alloys (Ref 5, 9). In literature it is reported that for the case of Ti and Nb added to high-Cr Fe-based alloys, the MC-type carbides (M representing the metal atoms) form prior to the M_7C_3 carbides, widening the solidification range of the alloy (Ref 5, 6). V in limited amount was observed to have a relatively low effect on the solidification path of Fe-based hardfacing alloys (Ref 5, 10). Moreover, V can form stable car-bides characterized by very high hardness, reaching up to 2800 HV (Ref 5, 11). Different morphologies of the V-rich carbides were observed to form depending on the chemical compositions of high-V cast irons, and on the cooling rate experienced during casting (Ref 7, 12, 13).

Considering that a fine carbide presence is a desired requisite in order to improve the toughness and wear resistance of the hardfacing alloys, in this research work the shape of vanadium carbides in V-bearing alloys was investigated as a function of composition and dilution. In a first step, high-V alloys were cast in alumina crucibles after calibrated graphite additions to a commercial Fe-C-B-Ni alloy aimed at producing

L. Rovatti, J.N. Lemke, A. Emami, and **M. Vedani**, Dipartimento di Meccanica, Politecnico di Milano, Milan, Italy; and **O. Stejskal**, Bernex Bimetallic s.r.o, Modrice, Czech Republic. Contact e-mail: ludovica.rovatti@polimi.it.

hypereutectic structure. The high-V alloys were characterized by differential scanning calorimetry, optical microscopy and scanning electron microscopy, and hardness measurements. In a second stage, V-rich alloy feedstock powders were molten directly inside steel crucibles in order to simulate the dilution phenomena occurring during deposition in real hardfacing

Table 1 Chemical compositions (wt.%) of the reference Fe-C-B-Ni and of the Fe-12V-Cr powder

Alloy code	C + B	Si	Mn	Cr	Ni	Mo	V
V0	4.3	2.06	0.54	0	3.93	0	0
Fe-12 V-Cr	2.8	0.9	0.5	5.2	0.6	1.25	12.2

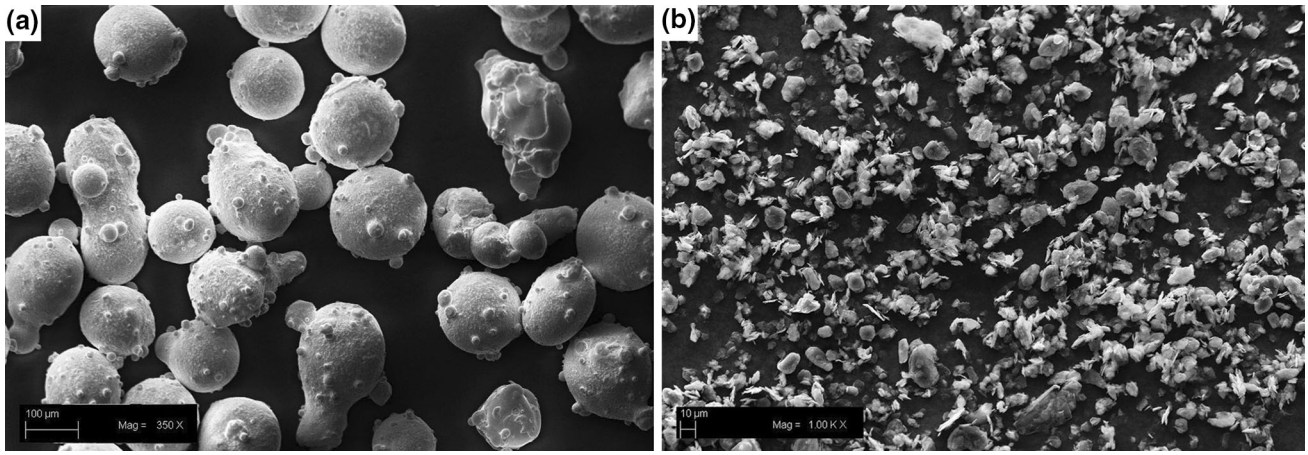

Fig. 1 SEM micrographs of the powders used in the casting experiments: Fe-12V-Cr (a) and graphite (b) powders

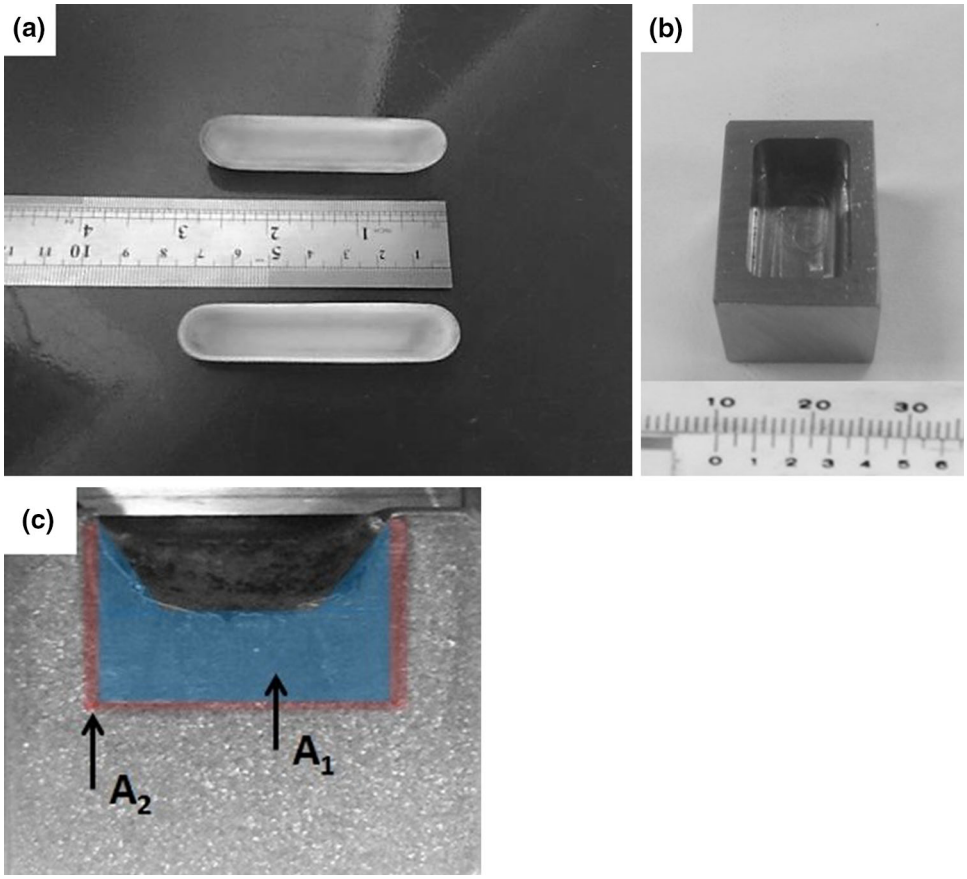

Fig. 2 Alumina crucible (a), steel crucible adopted for sample casting (b), and cross section of the steel crucible after casting (c)

processes such as spin casting, laser, or plasma transferred arc (PTA) cladding. Microstructure and hardness of the new V-rich hardfacing alloys after dilution were analyzed and discussed.

2. Materials and Experimental Procedures

The selected reference material was a commercial Fe-based C-B-Ni abrasion resistant powder alloy (hereafter labeled as V0 alloy), whose composition is given in Table 1, with a particle size in the range of 45 to 355 μm.

The composition of the starting alloy was modified with different additions of Fe-12V-Cr powder (25, 30, 40 wt.%) and of carbon in the form of graphite (1, 1.35, 1.5 wt.%) in order to cast hypereutectic alloys with enhanced microstructural and hardness properties.

As shown in Fig. 1, the atomised Fe-12V-Cr alloy powder featured a particle size in the range of 50 to 150 μm while graphite powders had a size lower than 45 μm. The powders were cast in alumina crucibles having a size of $70 \times 14 \times 10$ mm^3 (Fig. 2a). The compositions of the high-V hardfacing alloys obtained by blending the above powders are summarized in Table 2.

In a second stage, casting of alloys was realized in crucibles machined from C60 grade steel blocks using molds with a size of 25 mm in length, 15 mm in width, and 10 mm in depth, as shown in Fig. 2(b). In Fig. 2(c) is represented the transversal cross section of the steel crucible with the indication of the coating area (A_1), and the dilution area (A_2) caused by the partial melting of the substrate.

Table 2 Compositions (wt.%) of the experimental high-V alloys (balance Fe)

Alloy code	Preparation	C + B	Si	Mn	Cr	Ni	Mo	V
VG0	V0 + 40 Fe-12V-Cr	3.7	1.60	0.52	2.08	2.60	0.50	4.88
VG1	V0 + 25 Fe-12V-Cr + 1% graphite	4.89	1.75	0.52	1.29	3.07	0.31	3.02
VG2	V0 + 30 Fe-12V-Cr + 1.35% graphite	5.15	1.69	0.52	1.54	2.89	0.37	3.61
VG3	V0 + 40 Fe-12V-Cr + 1.5% graphite	5.14	1.57	0.52	2.05	2.56	0.49	4.81

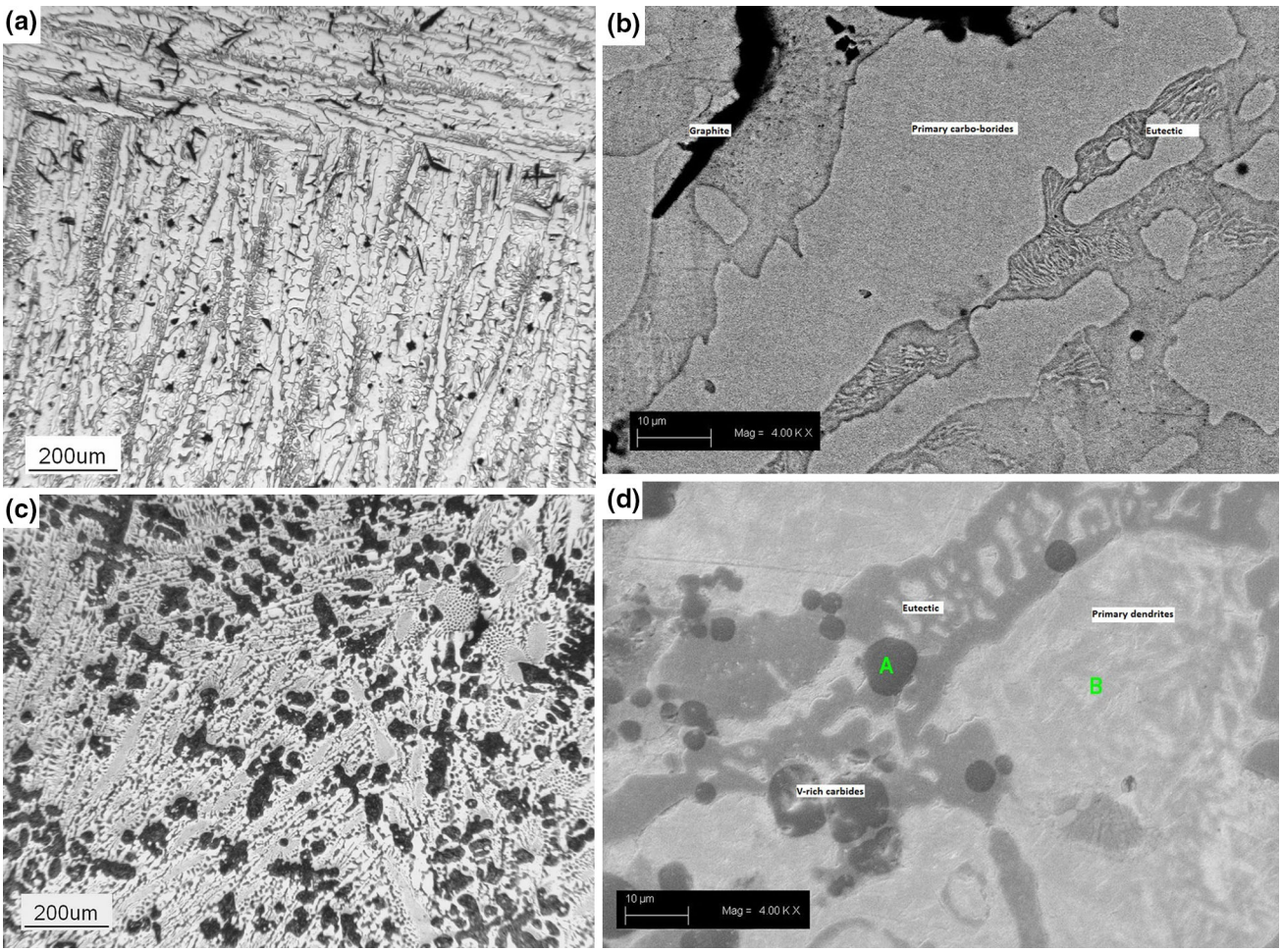

Fig. 3 Microstructure of the reference alloy V0 (a, b) and of the hypoeutectic V-bearing alloy VG0 (c, d)

Table 3 Microprobe chemical analysis related to positions given in Fig. 3(d) for the alloy VG0

Point analysis	Si	V	Cr	Mn	Ni	Mo	Fe
A	–	91.44	3.81	–	–	2.57	Bal.
B	2.8	0.74	1.32	–	3.83	–	Bal.

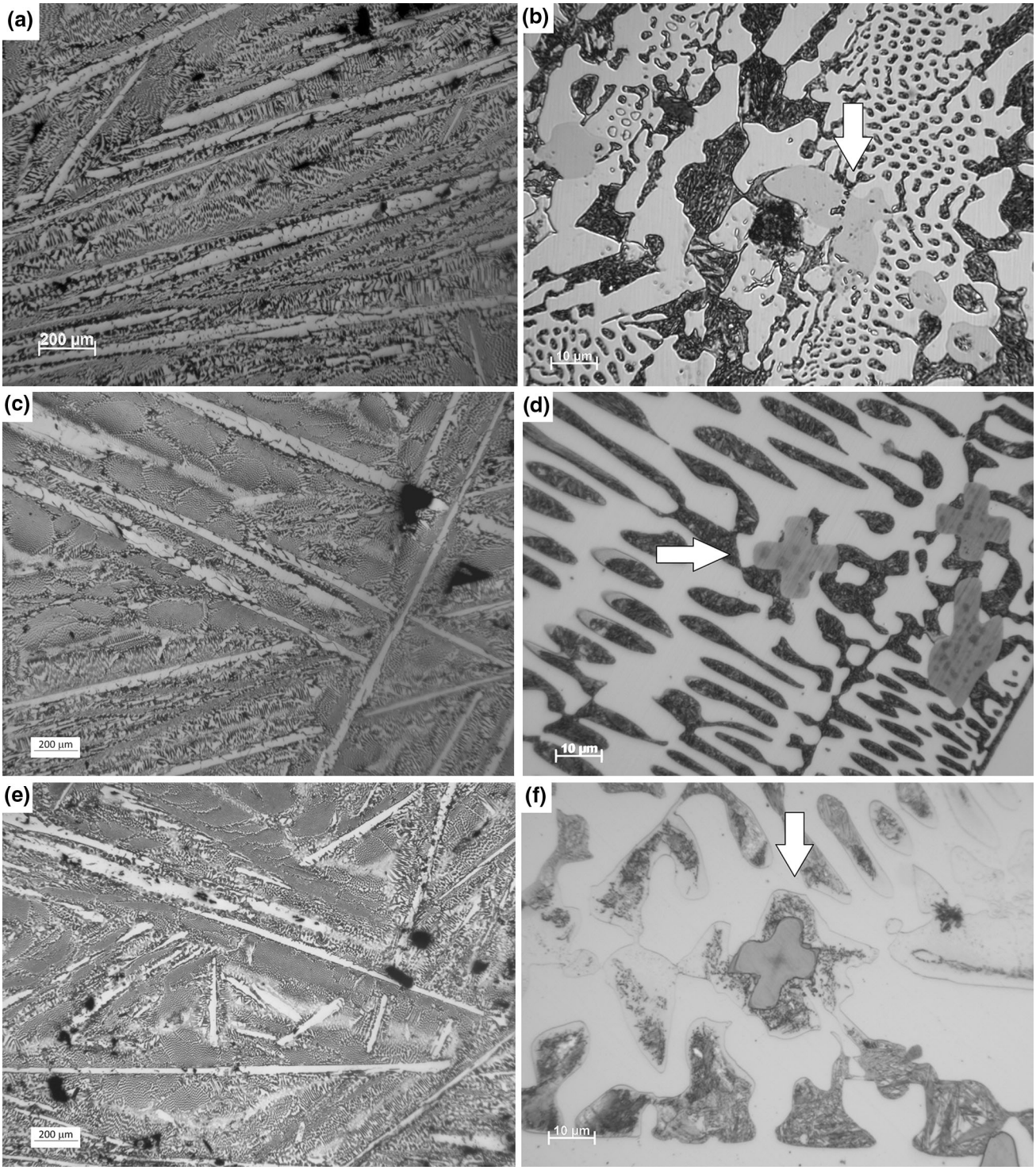

Fig. 4 Optical micrographs of the high-V alloys at two different magnifications: VG1 (a, b), VG2 (c, d), and VG3 (e, f). In figure b, d, and f, vanadium carbides are arrowed

Casting was performed in a furnace equipped with a flow of Ar as shielding gas. Microstructural investigations were carried out after metallographic polishing of the transversal sections of the cast alloys and etching with Nital 3% using an optical microscope (OM) by a Leitz Aristomet and a scanning electron microscope (SEM) by Zeiss EVO 50. Image analysis was adopted for measuring the carbide size, phase volume fraction, and macroscopic dilution (d) that was evaluated by the formula:

$$d = \frac{A_2}{A_1 + A_2}, \qquad \text{(Eq 1)}$$

where A_1 is the coating area after casting and A_2 is the molten substrate area (Fig. 2c) (Ref 14). Macrohardness tests were carried out using a Vickers equipment with a load of 981 N on the indenter, while microhardness was performed with load of 19.6 N to measure hardness profiles across the transition zone between substrate and cast alloys molten in steel crucibles.

Differential scanning calorimetry (DSC) tests were carried out to measure liquidus and solidus temperatures of the alloys. The thermograms were generated by imposing a heating ramp up to 1250 °C at a rate of 30 °C/min, 15 min holding at maximum temperature followed by a cooling step at the same rate in Ar atmosphere. In particular, heat flow was recorded as a function of temperature and by analysing the cooling curves, the offset and onset points of the melting and solidification ranges were determined.

3. Results and Discussion

3.1 Microstructure of the Alloys Cast in the Alumina Crucibles

The microstructure of the reference alloy is depicted in Fig. 3(a) and (b). Previous research showed that the Fe-based reference alloy is characterized by primary columnar carboborides $M_3(C,B)$, by limited graphite flakes and by the eutectic (Ref 10). After the addition of 40% of Fe-12V-Cr, the alloy shifted to a hypoeutectic composition characterized by the presence of primary dendrites of Fe-based solid solution with bainitic-martensitic structure and of near-spherical V-rich carbides mainly detected within the eutectic structure (see Fig. 3d) (Ref 10).

In particular, microprobe analyses (given in Table 3) demonstrated that the nearly spherical carbides mainly contains V and a small amount of Cr and Mo.

In order to balance the depletion of carbon due to dilution and to produce modified hypereutectic alloys containing more than 3 wt.% of vanadium, increasing graphite levels were considered (Table 2). As it can be observed in Fig. 4, all the new alloys showed a hypereutectic solidification. In particular, the addition of 1.5 wt.% of graphite shifted the hypoeutectic microstructure of the alloy VG0 to the hypereutectic structure of the alloy VG3. A summary of the volume fraction of the $M_3(CB)$ columnar primary phases related to the hypereutectic alloys and of the metallic dendrites for the alloy VG0 measured by image analysis is reported in Table 4.

The volume fraction results show that the graphite amounts were correctly chosen for producing the new hypereutectic alloys with similar amount of primary carbo-borides.

Moreover, in the high-magnification optical micrographs, the presence of dendritic vanadium carbides can be detected (see arrowed phases in Fig. 4b, d, f).

The presence of petal-like V-rich carbides, with an average size higher than 10 μm, was observed in all the new V-containing alloys VG1, VG2, and VG3 cast in alumina crucibles (see Fig. 4b, d, f). Moreover, comparing the alloys VG0 and VG3 characterized by the same vanadium content, it can be concluded that the V-rich carbides assumed a petal-like morphology, after the graphite addition, when the alloy solidification became of hypereutectic type (compare Fig. 3d and 4f). The same morphological change in the VC carbides was observed by K. Tokaji et al. in high Cr-V-Ni cast irons after increasing the carbon level and preserving the V/C ratio (Ref 13).

The formation of the petal-like carbides can be related to the higher carbon concentration of the VG3 alloy, in comparison to the VG0 alloy, that induced the formation of the dendritic V-rich phases (Ref 12, 15). In Fig. 5 the backscattered electron (BSE) micrograph of the VG3 alloy shows the presence of petal-like phases within the Fe-rich primary columnar carboborides, supporting the hypothesis of the V-rich carbide formation prior to the eutectic transformation.

In order to compare the hardness of new V-bearing alloys with the reference alloy, macrohardness tests were performed. The hardness results are summarized in the chart of Fig. 6.

The results of the macrohardness tests showed a significant hardness increase already after the graphite and 3 wt.% of vanadium additions, represented by the alloy VG1. The hardness of the alloy VG0 was significantly lower compared to that of the high-V hypereutectic alloys due to the lack of primary hard phases.

To analyze the solidification behavior of the new V-rich alloys, DSC tests were performed. The DSC curves related to

Table 4 Volume fraction of primary phases in the alloys cast in alumina crucibles

Alloy code	Volume fraction, %	Type of primary phase
V0	46.66	Carbo-borides
VG0	30.30	Metallic dendrites
VG1	17.30	Carbo-borides
VG2	19.80	Carbo-borides
VG3	17.30	Carbo-borides

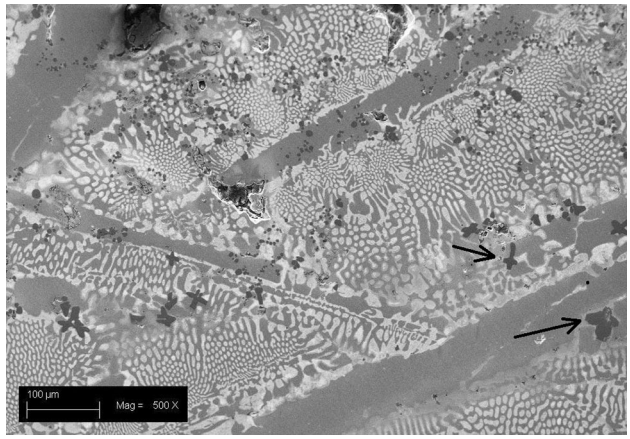

Fig. 5 BSE-SEM micrograph of alloy VG3. The petal-like carbides inside the primary columnar phases are arrowed

the alloys V0, VG0, VG1, and VG3 are depicted in Fig. 7. Two main peaks were identified in all the cooling curves. In particular, the highest exothermic peaks of the curves are related to eutectic solidification while smaller peaks at higher temperatures are connected to the primary carbo-borides $M_3(C,B)$ formation in the case of the hypereutectic alloys (V0, VG1, and VG3) and to Fe-based solid solution dendrites for the hypoeutectic alloy (VG0). Moreover, the cooling curves reveal that the transformation temperatures increase for the V-containing alloys. The same shift in the eutectic temperature was obtained by Filipovic et al. through DTA measurements in high Cr cast iron alloyed with vanadium (Ref 16).

The melting and solidification ranges measured for the investigated alloys are summarized in Table 5. As it can be observed, the hypereutectic V0, VG1, and VG3 alloys have a very similar and fairly narrow solidification range while the VG0 alloy shows a much wider solidification range due to the hypoeutectic nature of the alloy (Ref 10).

It can be noticed that the solidification range is a key parameter for the deposition of hardfacing materials. Alloys with too wide solidification gap, in fact, are more prone to hot cracking (Ref 17).

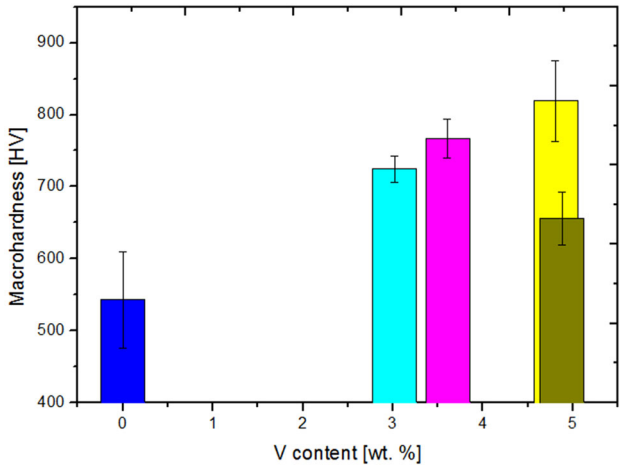

Fig. 6 Hardness values of the alloys V0, VG0, VG1, VG2, and VG3 cast in alumina crucibles

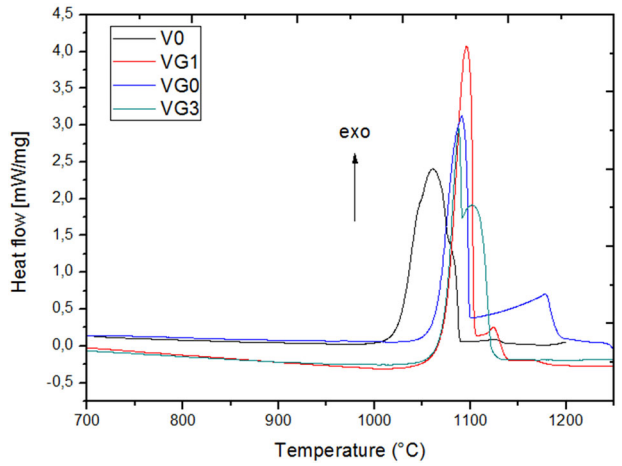

Fig. 7 DSC cooling curves of the reference alloy V0 in comparison with the V-containing alloys VG0, VG1, and VG3

3.2 Casting of Reference Alloy and of the V-bearing Alloys in Steel Crucibles

Figure 8 shows the representative microstructure observed in the transversal sectioned steel crucibles at different positions from the original interface of the V-bearing VG1 alloy and of the reference alloy V0. It can be noticed in Fig. 8(e) and (f) that both alloys show a hypoeutectic microstructure, starting from the interface up to the center, due to dilution effects induced by the Fe-rich substrate. In the center and at the top of the cast samples, where dilution had a much lower effect, a near-eutectic and hypereutectic structure were, respectively, detected (Fig. 8a-d).

Similar effects of dilution on the microstructure were also detected in alloys VG2 and VG3 prepared through the same casting procedure. In order to show the microstructural evolution of the diluted alloys, the content of the primary phases was measured in different area of the steel crucibles (see Table 6).

As expected, the primary carbo-boride volume fraction at the top of the steel crucibles was lower than the value measured in the same alloys cast in the alumina (see Table 4). Moreover, comparing the values reported in Table 5 and 6, the amount of primary dendrites at the interface was consistent with the starting carbo-boride content of the undiluted alloys. The dilution was measured according to the formula (1), obtaining values higher than 10% for all the analyzed alloys, as reported in Table 6. The dilution level was high enough to shift the hypereutectic structure to the hypoeutectic one, due to the relatively low amount of interstitial alloying elements (see Table 1 and 2). In fact, the dilution phenomenon depends not only on deposition process parameters, but also on composition of the hardfacing alloy (Ref 10).

Furthermore, the V-bearing alloys cast into steel crucibles were deeply analyzed in order to investigate the V-rich carbide distribution within the microstructure. Starting from a distance

Table 5 Melting and solidification ranges of the investigated alloys

	Heating			Cooling		
Alloy	***T* onset, °C**	***T* offset, °C**	**Δ*T*, °C**	***T* onset, °C**	***T* offset, °C**	**Δ*T*, °C**
V0	1090.1	1149.1	59	1088.2	1025.6	62.6
VG0	1135.6	1236	100.4	1191.6	1064.5	127.1
VG1	1102.4	1155.2	52.8	1139.2	1073.3	65.9
VG3	1114.4	1163.6	49.2	1122.2	1071.9	50.3

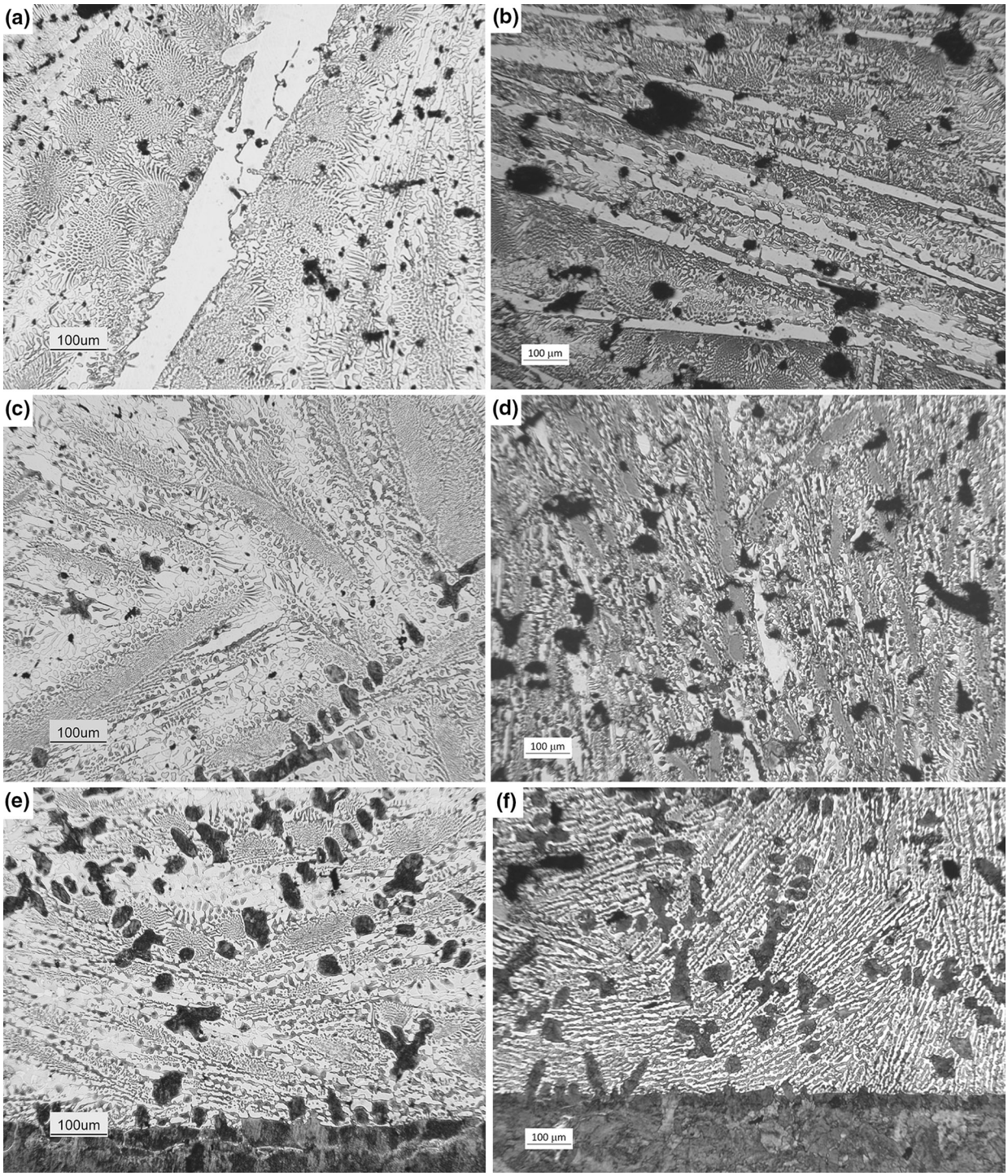

Fig. 8 Optical micrographs of the reference alloy V0 (a, c, e) in comparison with alloy VG1 (b, d, f) cast in the steel crucible at three different positions: top part of ingot (a, b), center of ingot (c, d), and interface with substrate (e, f)

Table 6 Primary phase volume fraction and macroscopic dilution for alloys cast in steel crucibles

Alloy code	Metallic dendrites (%) at the interface	Carbo-borides (%) in the middle	Carbo-borides (%) at the top	Dilution, %
V0	9.98	13	25.15	13.35
VG1	19.18	8.47	15.41	10.04
VG2	22.84	7.01	17.02	12.54
VG3	26.25	8.66	13.33	11.46

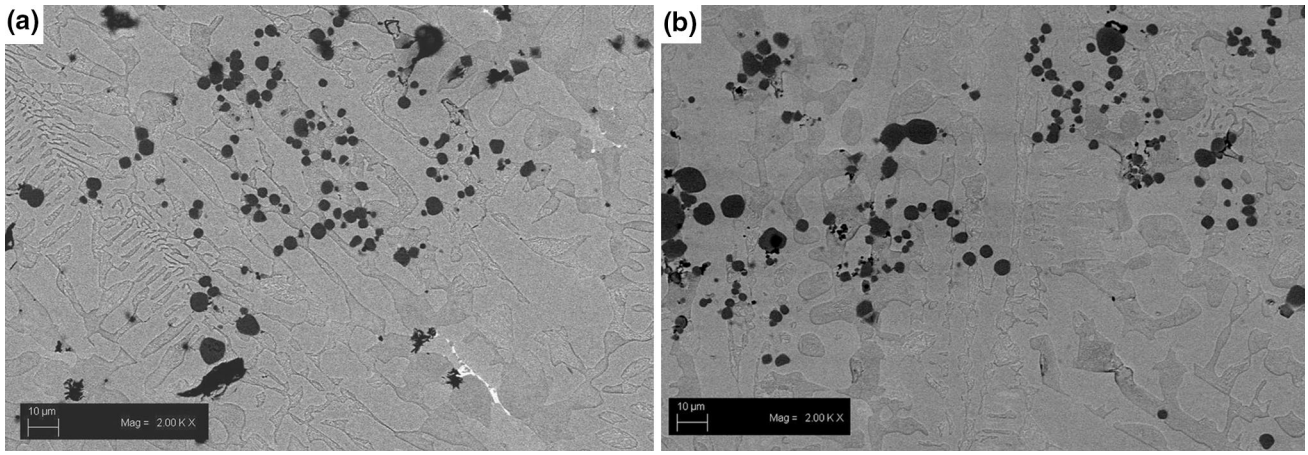

Fig. 9 SEM micrographs of the alloys VG1 (a) and VG3 (b) in the central part of the steel crucible

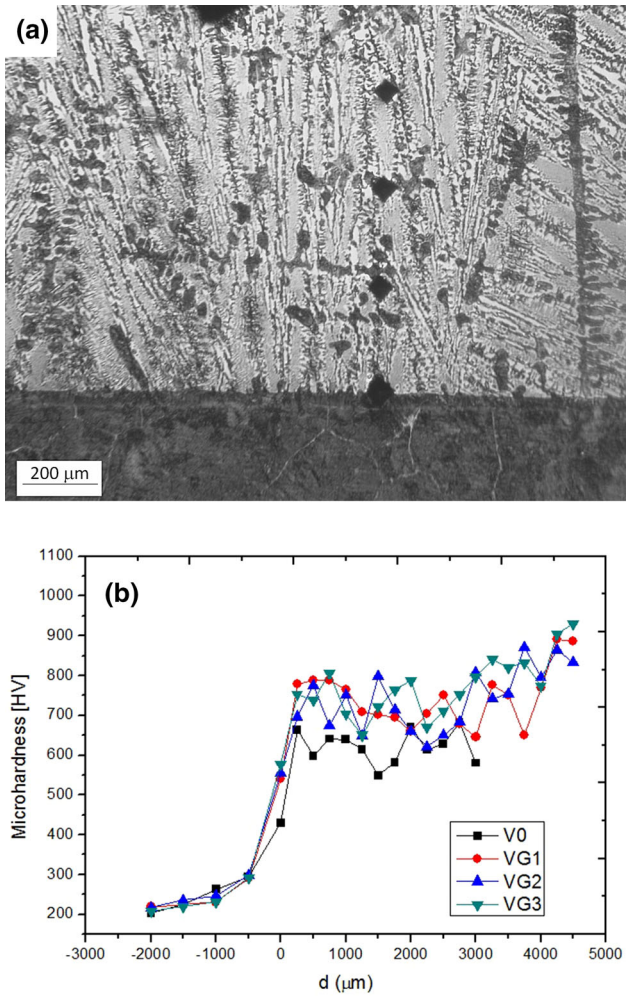

Fig. 10 Transversal section of the alloy VG3 molten in steel crucible (a) and hardness profiles of the high-V alloys in comparison to the reference alloy (b)

of about 500 µm from the interface, nearly-globular V-rich carbides having an average size of 3 µm were observed in the eutectic structure, as shown by BSE-SEM micrographs reported in Fig. 9.

Comparing the same V-rich alloys cast in alumina and steel crucibles, it can be clearly seen that in the case of alloys cast in the steel crucibles (affected by dilution) the carbide morphology is near-globular, while, the carbides found in undiluted alumina crucibles featured a petal-like shape.

From SEM investigation it was also revealed that the coating/substrate interface region was free of V-rich carbides. This phenomenon was detected in all the diluted V-bearing alloys and it can be related to the decreased carbon level in this area but also to a segregation of the V-rich carbides due to expected differences in density. Literature data suggest that vanadium carbides feature a density of about 5.7 g/cm^3 while the alloy of about 7 g/cm^3 (Ref 18). This difference could justify the preferential upward flow of the carbides in the melt by several hundreds of µm. This effect could be highlighted in the alloys molten in steel crucible due to the difference in cooling rate between the two type of crucibles.

Microhardness profiles were performed on the three V-bearing hypereutectic alloys and compared to the reference alloy after casting in steel crucibles. The graphs reported in Fig. 10, show an improvement in hardness properties in all the V-bearing alloys even considering the dilution effects produced by melting in the steel crucibles.

Moving toward the interface with the substrate, it can be observed that for all the alloys the hardness trend is decreasing, as expected by the microstructural modifications previously discussed (Fig. 8). However, it is important to note that the V-bearing alloys showed higher hardness values than the reference alloy already at a distance of 500 µm from the interface. This result is due to the presence of the V-rich carbides in this area. Moreover, in the top section of the coatings, characterized by the hypereutectic microstructure and by the presence of the hard carbides, the hardness values increased above 800 HV. The hardness fluctuations observed in all profiles are due to the porosity and effects of coarse carbides of the cast alloys.

4. Conclusions

The experimental approach carried out in this research allowed primarily to analyze V-rich alloys in the as cast condition after calibrated graphite additions and, successively,

to isolate the effect of dilution induced by melting atomized powders on plain carbon steel. The main conclusions can be summarized as follows:

- The microstructure of the new hypereutectic alloys was characterized by the presence of dendritic V-rich carbides, $M_3(CB)$ columnar phases and eutectic structure.
- In the case of the V-rich hypereutectic alloys the transformation temperatures shifted to higher temperatures and the solidification gap remained close to that of the reference alloy.
- It was measured a significant improvement in hardness in the new hardfacing alloys compared to the reference alloy, due to the presence of the hard V-rich carbides. In the hypereutectic alloys even a fairly low amount of V (3 wt.%) could promote a significant increase in hardness while further addition of V did not generate any relevant improvement.
- The lack of carbon caused by the melting of the new alloys in the steel crucibles induced the formation of near-spherical V-rich carbides and the transition from the hypereutectic to the hypoeutectic microstructure at the interface with the substrate, corresponding to a level of dilution higher than 10%.

The analysis of the dilution effects on the hardfacing alloys can be significant for the optimization of the chemical compositions and of the tribological properties along the full thickness of the protective coating.

Acknowledgment

The present research was financed under the research project DEBACOAT (development of high-performance barrels with innovative gradient coatings) funded by the European Commission under the call FP7-SME-2012 (Project ID: 315417).

References

1. H. Berns, Comparison of Wear Resistant MMC and White Cast Iron, *Wear*, 2003, **254**, p 47–54
2. E.O. Correa, N.G. Alcantara, D.G. Tecco, and R.V. Kumar, The Relationship Between the Microstructure and Abrasive Resistance of a Hardfacing Alloy in the Fe-Cr-C-Nb-V System, *Metall. Mat. Trans. A*, 2007, **38**(8), p 1671–1680
3. T. Lucey, R. Wuhrer, K. Moran, M. Reid, P. Huggett, and M. Cortie, Interfacial Reactions in White Iron/Steel Composites, *J. Mater. Proc. Techn.*, 2012, **212**(11), p 2349–2357
4. I. Hemmati, V. Ocelík, and J.Th.M. De Hosson, Dilution Effects in Laser Cladding of Ni–Cr–B–Si–C Hardfacing Alloys, *Mater. Lett.*, 2012, **84**, p 69–72
5. R.J. Chung, X. Tang, D.Y. Li, B. Hinckley, and K. Dolman, Microstructure Refinement of Hypereutectic High Cr Cast Irons Using Hard Carbide-Forming Elements, *Wear*, 2013, **301**, p 695–706
6. X. Zhi, J. Xing, H. Fu, and Y. Gao, Effect of Titanium on the As-Cast Microstructure of Hypereutectic High Chromium Cast Iron, *Mat. Charact.*, 2008, **59**, p 1221–1226
7. R. Kesri and M. Durand-Charre, Phase Equilibria, Solidification and Solid-State Transformations of White Cast Irons Containing Niobium, *J. Mater. Sci.*, 1987, **22**, p 2959–2964
8. X.H. Wang, F. Han, X.M. Liu, S.Y. Qu, and Z.D. Zou, Effect of Molybdenum on the Microstructure and Wear Resistance of Fe-based Hardfacing Coatings, *Mater. Sci. Eng. A*, 2007, **489**, p 193–200
9. A. Röttger, S. Weber, and W. Theisen, Supersolidus Liquid-Phase Sintering of Ultrahigh-Boron High-Carbon Steels for Wear-Protection Applications, *Mater. Sci. Eng. A*, 2012, **532**, p 511–521
10. L. Rovatti, R. Casati, A. Emami, N. Lecis, O. Stejskal, C. Andrianopoli, and M. Vedani, Effect of Vanadium on Microstructure and Wear Behaviour of Fe Based C-B–Ni Hardfacing Alloy, *Int. J. Cast. Met. Res.*, 2015, **28**(4), p 201–207
11. D.A. Porter, K.E. Easterling, and M.Y. Sherif, *Phase Transformations in Metals and Alloys*, 3rd ed., CRC Press, London, 2009
12. K. Tokaji, T. Horie, and Y. Enomoto, Effect of Microstructure and Carbide Spheroidization on Fatigue Behavior in High V-Cr-Ni Cast Irons, *Int. J. Fatigue*, 2006, **28**, p 281–288
13. E. Fras, M. Kawalec, and H.F. Lopez, Solidification Microstructures and Mechanical Properties of High-Vanadium Fe–C–V and Fe–C–V–Si Alloys, *Mat. Sci. Eng. A*, 2009, **524**, p 193–203
14. Y. Huang, Characterization of Dilution Action in Laser-Induction Hybrid Cladding, *Opt. Laser Technol.*, 2011, **43**, p 965–973
15. G.I. Sil'man, Phase Diagram of the Fe-C-V System and Its Application to Metallography of Steels and Cast Irons, *Met. Sci. Heat Treat.*, 1992, **34**(11), p 665–670
16. M. Filipovic, Z. Kamberovic, and M. Korac, Solidification of High Chromium White Cast Iron Alloyed with Vanadium, *Mater. Trans.*, 2011, **52**(3), p 386–390
17. J. Campbell, *Castings*, 2nd ed., Butterworth Heinemann, Oxford, 2003
18. H. Fua, Q. Xiao, and J. Xing, A Study of Segregation Mechanism in Centrifugal Cast High Speed Steel Rolls, *Mat. Sci. Eng.*, 2008, **A479**, p 253–260